



# UNIVERSITY OF TWENTE.

Faculty of Electrical Engineering,  
Mathematics & Computer Science

## Improving efficiency of tri-state boost converters for audio applications using dynamic freewheeling

S.P. de Vos  
B.Sc. Thesis  
June 2018



---

**Supervisors:**

dr.ir. R.A.R. van der Zee

C.E. Lokin MSc

dr. ir. A.B.J. Kokkeler

Integrated Circuit Design Group  
Faculty of Electrical Engineering,  
Mathematics and Computer Science  
University of Twente  
P.O. Box 217  
7500 AE Enschede  
The Netherlands

---

## Abstract

The present solution for high-power portable audio is to use a boost converter followed by a class-D amplifier. This report investigates driving a speaker directly with a boost converter to increase efficiency. The challenge is that a boost converter has an inverse response at high frequencies, limiting audio quality.

This report combines two existing approaches: A bridge configuration is used to remove direct current into the speaker. Combined with a tri-state topology that eliminates the inversion, at the cost of higher inductor current and losses.

A new control scheme is proposed that limits excess inductor current, resulting in better efficiency. A parameter sweep was done to show that using the dynamic tri-state design, excess current can be traded for audio quality, where a sweet spot can be found that saves energy without degrading performance significantly.

Simulations show that the proposed scheme allows increased loop gain, resulting in a THD of 0.51%. It is only 7 percent point less efficient than a conventional boost converter. This makes it an appealing alternative to a separate boost converter and amplifier.

# Contents

<b>1</b>	<b>Introduction</b>	<b>4</b>
<b>2</b>	<b>Tri-state Bridge Boost Converter</b>	<b>6</b>
2.1	Bridge Boost Converter . . . . .	7
2.2	Tri-state boost converter . . . . .	12
2.3	Simulation . . . . .	13
<b>3</b>	<b>Dynamic Tri-state Bridge Boost Converter</b>	<b>16</b>
3.1	High-pass filter design . . . . .	17
3.2	PWM generation . . . . .	19
3.3	Simulation . . . . .	20
<b>4</b>	<b>Discussion</b>	<b>25</b>
4.1	Feedback stability . . . . .	25
4.2	Parameter Sweep . . . . .	25
4.3	Efficiency . . . . .	26
<b>5</b>	<b>Conclusion</b>	<b>28</b>
<b>6</b>	<b>Appendix</b>	<b>29</b>
<b>A</b>	<b>Single-ended dynamic predistortion</b>	<b>29</b>
<b>B</b>	<b>Static bridge Predistortion</b>	<b>30</b>
<b>C</b>	<b>Peak detector</b>	<b>33</b>
<b>D</b>	<b>LTspice schematics</b>	<b>35</b>

# 1 Introduction

In recent years, switching mode audio amplifiers have been on the rise, driven by an explosion of portable electronics that get smaller and more powerful by the year. Switching mode amplifiers are a great match for this application due to their compactness and efficiency. However, these portable electronics such as wireless Bluetooth speakers, smartphones, and even smartwatches all operate on low voltages. Commonly a single lithium cell, providing merely 3.7V.

This poses a problem for audio amplifiers, as it provides little headroom and even less output power, severely limiting volume. Assuming rail-to-rail sinusoidal output of  $\frac{3.7}{\sqrt{2}} = 2.6$  V into a  $4\Omega$  load, this produces only  $\frac{2.6^2}{4} = 1.71$  W. So clearly a higher voltage is needed. The conventional solution is to put a boost converter in front of the amplifier. This is however not good for efficiency, as both switching devices have losses. If both devices were 85% efficient, the total efficiency would be as low as  $0.85 \cdot 0.85 = 72\%$ .

A more efficient approach would be to drive the speaker directly with the boost converter by modulating its duty cycle. However, this is challenging due to highly non-linear behaviour and a right half-plane zero (RHPZ) in the control-to-output transfer function, which limits the amount of voltage feedback that can be used to eliminate non-linearities and improve audio quality.

A simple boost converter is pictured in fig. 1 that alternates between charging the inductor current via  $M_1$  and discharging the inductor current into  $C$  via  $M_2$ . The output voltage is determined by the duty cycle, the percentage of time that  $M_1$  is conducting.

A problem arises when the duty cycle is changed very quickly, for example as in music. An increase in duty cycle means that  $M_1$  conducts longer, and  $M_2$  conducts shorter. So over time, the inductor will be charged more. However, the inductor current changes rather slowly, and the reduced time that  $M_2$  conducts instantaneously reduces the current into  $R$ .

So the problem is that when a step in duty cycle happens (fig. 2), the output first makes an inverse response before the inductor is charged up. This means that when feedback is applied, the system is unstable, because it gives positive feedback for high frequencies.

A solution to this inverse RHPZ behavior is the use of a tri-state boost converter [7], in which a third switch is introduced around the inductor and the duty cycle of  $M_2$  is kept constant. This means that a change in inductor current results in a directly proportional change in output current.

While the tri-state solution provides excellent linearity and frequency response, it is not immediately suitable for the intended application of portable audio. Most importantly, efficiency is degraded tremendously, having up to nine times more power loss than a conventional boost converter [6].

This completely defeats the purpose of replacing a boost converter in combination with a class-D amplifiers. In order to be usable in this context, an increase of efficiency is needed such that it is more efficient than the combined efficiency of a separate converter and amplifier.

In this report, the goal is to make the tri-state boost converter suitable for portable audio applications. This is done in two ways. First the boost converter is put in bridge to removed direct current, increase maximum voltage, improve linearity, and reduce distortion.

Figure 1: Basic boost converter

Then, a new approach is presented that improves efficiency. It will be shown that efficiency is proportional to the duty cycle of the introduced freewheel switch, and a new control scheme is proposed that minimizes this duty cycle, thereby increasing efficiency.

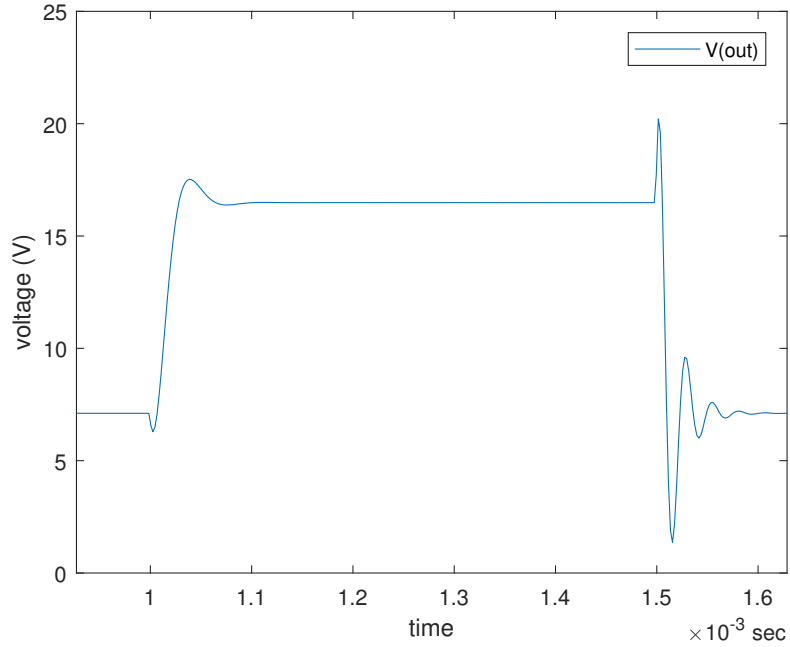


Figure 2: Basic boost converter step response

## 2 Tri-state Bridge Boost Converter

The problems with driving a speaker with a boost converter are manifold. Besides the fundamental problem of the RHPZ, there are a few other practicalities that make a normal boost converter completely unsuitable for audio. To see why, the voltage gain of a normal boost converter will be derived.

In figure fig. 1 a classical boost converter is displayed, which has the following well known relation between duty cycle  $D$ , source voltage  $V_g$  and output voltage  $V_R$ . The gain is derived by calculating the change in current during one switching period  $T$  when  $M_1$  is on and  $M_2$  is off ( $\Delta I_{L,gnl}$ ), and when  $M_2$  is on and  $M_1$  is off ( $\Delta I_{L,fd}$ ). Then, for a steady-state situation, the total change in current must be 0. It is important for the rest of this report to note that the gain is independent of the load and switching period  $T$ .

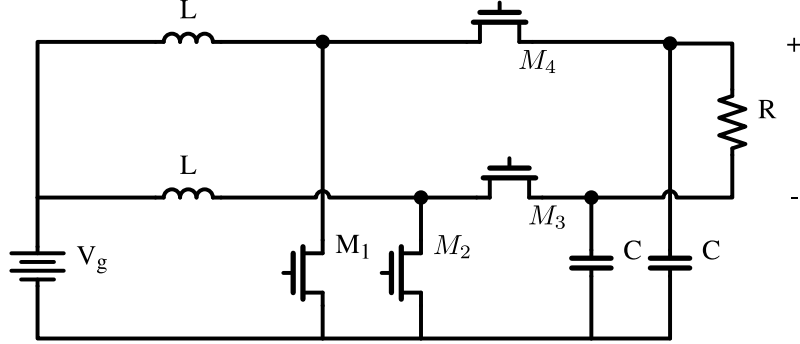


Figure 3: Full bridge boost converter

$$\Delta I_{L,gnd} = \frac{1}{L} \int_0^{DT} V_g dt \quad (1)$$

$$\Delta I_{L,gnd} = \frac{DT}{L} V_g \quad (2)$$

$$\Delta I_{L, fwd} = \frac{1}{L} \int_{DT}^T (V_g - V_R) dt \quad (3)$$

$$\Delta I_{L, fwd} = \frac{T}{L} (1 - D)(V_g - V_R) \quad (4)$$

$$0 = \Delta I_{L,gnd} + \Delta I_{L, fwd} \quad (5)$$

$$0 = \frac{DT}{L} V_g + \frac{T}{L} (1 - D)(V_g - V_R) \quad (6)$$

$$\frac{V_R}{V_g} = \frac{1}{1 - D} \quad (7)$$

From eq. (7), two things become clear. First of all, the output voltage has a highly non-linear relation to the duty cycle. But maybe more importantly for audio is that the voltage scales between  $V_g$  and  $\infty$ , meaning that a large DC is applied to the speaker.

## 2.1 Bridge Boost Converter

To solve both of these issues, two boost converters can be put in a bridge configuration as explored in [1] and [4] and displayed in fig. 3. Using a bridge configuration results in the following relation between duty cycle and output voltage. As plotted in fig. 4, this relation is both symmetric around 0 V and much more linear than a single boost converter.

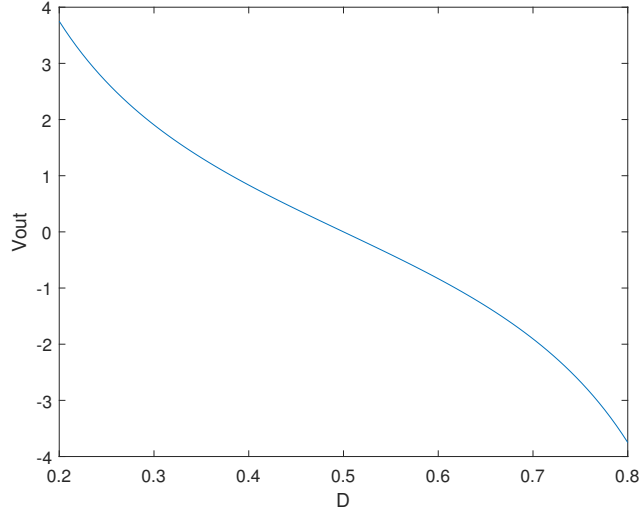


Figure 4: Bridge control-to-output gain

$$V_R = \frac{1}{D} - \frac{1}{1-D} \quad (8)$$

$$V_R = \frac{(1-D) - D}{D(1-D)} \quad (9)$$

$$V_R = \frac{1-2D}{D-D^2} \quad (10)$$

$$(11)$$

So far the analysis has only been concerned with static behavior. The boost converter RHPZ is a dynamic phenomenon, so a dynamic analysis of the bridge configuration is required. Dynamic analysis of a boost converter is challenging due to high-frequency switching and non-linear behavior. However, assuming the switching ripple is relatively small, an average switching model can be used. To find the transfer function, the system needs to be linearized around an operating point using a small-signal equivalent circuit.

The full bridge transfer function is a fourth order system that was derived using a computer program, and does not provide further insights as no practical analytic expression exists for the poles and zeros. The full bridge equation is provided below.

$$\frac{(-C I_{L,1} L^2 R - C I_{L,2} L^2 R) s^3 + (C D_2 L R V_2 - C D_1 L R V_1) s^2 + (-I_{L,2} L R D_1^2 - I_{L,1} L R D_2^2) s + D_1^2 D_2 R V_2 - D_1 D_2^2 R V_1}{(C^2 L^2 R) s^4 + (2 C L^2) s^3 + (C L R D_1^2 + C L R D_2^2) s^2 + (L D_1^2 + L D_2^2) s + D_1^2 D_2^2 R} \quad (12)$$

In the following analysis, a simplification is made by assuming a bridge of boost converters can be modelled as a biased half-bridge. This assumes the behaviour is symmetric around the bias point, which is not necessarily the case because each half-bridge output scales with  $\frac{1}{1-D}$  and because the frequency response depends on  $D$ . So verification of this model is needed.

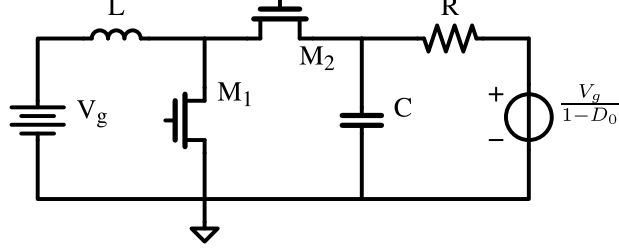


Figure 5: Boost converter half bridge model

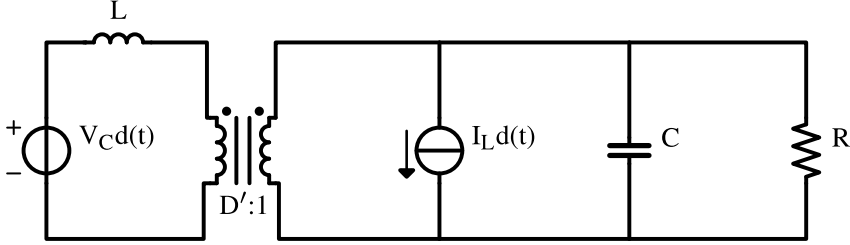


Figure 6: Boost converter SSEC

A small signal analysis is performed by analyzing a half bridge with a biasing voltage source, operating around a duty cycle  $D_0$ , as displayed in fig. 5. Note that  $R$  of the half-bridge is half that of the full bridge, as should be expected.

A small-signal equivalent circuit (SSEC) with averaged switching will be used to derive the transfer function of the bridge configuration in fig. 5. The SSEC is taken around large-signal output voltages  $V_R$  (differential),  $V_C$  (one-sided), inductor current  $I_L$ , and complementary duty-cycle  $D' = 1 - D$  with the corresponding small-signal variations  $\hat{v}$ ,  $\hat{i}$  and  $\hat{d}$ .

The SSEC is derived as discussed in [2], resulting in fig. 6. Due to shorting the DC sources, this is equivalent to the SSEC of a standard boost converter in [2] (fig. 7.17b), but it should be noted that the large-signal voltages and currents are different due to the voltage source in fig. 5. Superposition can now be used to find contributions from the  $\hat{d}$ -dependant sources on the load  $R$ . The superposition circuits are displayed in fig. 7.

Using fig. 7, the small-signal variations  $\hat{v}_1(s)$  (top circuit) and  $\hat{v}_2(s)$  (bottom circuit) of  $V_C$  due to variations  $\hat{d}(s)$  of  $D$  can be calculated. Using superposition of  $\hat{v}(s) = \hat{v}_1(s) + \hat{v}_2(s)$ , the total transfer function  $H(s) = \frac{\hat{v}(s)}{\hat{d}(s)}$  can be calculated.

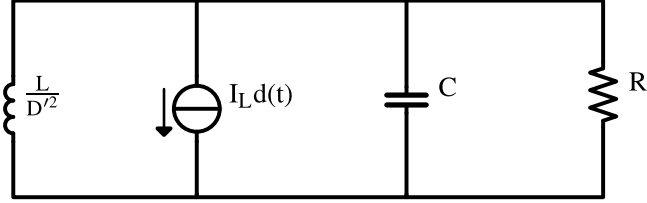
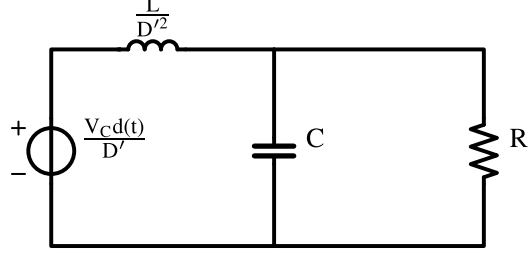


Figure 7: Super position of the two  $\hat{d}$ -dependant sources

$$\frac{\hat{v}_1(s)}{\hat{d}(s)} = -I_L \left( \frac{sL}{D'^2} \parallel \frac{1}{sC} \parallel R \right) \quad (13)$$

$$= -I_L \frac{sLR}{RD'^2 + sL + s^2RLC} \quad (14)$$

$$\frac{\hat{v}_2(s)}{\hat{d}(s)} = \frac{V_C}{D'} \frac{(R \parallel \frac{1}{sC})}{\frac{sL}{D'^2} + (R \parallel \frac{1}{sC})} \quad (15)$$

$$= V_C \frac{D'R}{RD'^2 + sL + s^2RLC} \quad (16)$$

$$\frac{\hat{v}(s)}{\hat{d}(s)} = \frac{\hat{v}_1(s) + \hat{v}_2(s)}{\hat{d}(s)} \quad (17)$$

$$= \frac{-sI_LLR + V_CD'R}{RD'^2 + sL + s^2RLC} \quad (18)$$

$$= \frac{V_C}{D'} \frac{1 - s\frac{I_LL}{V_CD'}}{1 + s\frac{L}{RD'^2} + s^2\frac{LC}{D'^2}} \quad (19)$$

Up until this point, the transfer function is identical to that of a normal boost converter, because it still depends on the large-signal voltages and currents. As a final step, the large-signal  $V_C$  and  $I_L$  in fig. 5 can be expressed in source voltage  $V_g$ , duty cycles  $D$ ,  $D_0$  and component values  $R$ ,  $L$ ,  $C$ , resulting in the final transfer function.

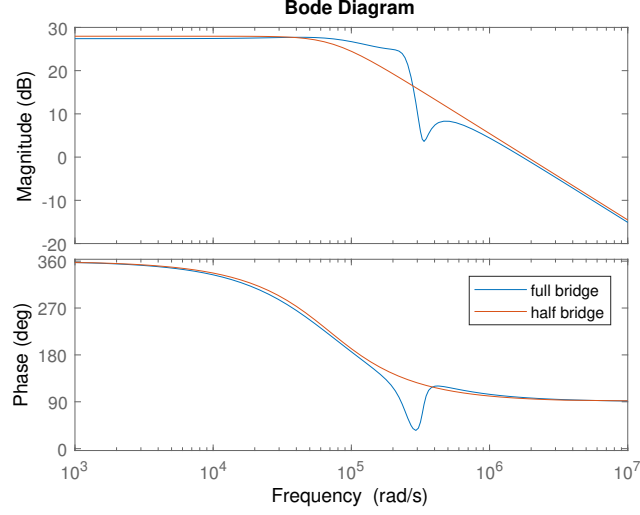


Figure 8: Bode plot of the full bridge and half bridge simplification

$$D'_0 = 1 - D_0 \quad (20)$$

$$V_C = \frac{V_g}{D'} \quad (21)$$

$$I_R = \frac{\frac{V_g}{D'} - \frac{V_g}{D'_0}}{R} \quad (22)$$

$$= \frac{V_g}{D'R} \left(1 - \frac{D'}{D'_0}\right) \quad (23)$$

$$I_L = \frac{V_g}{D'^2 R} \left(1 - \frac{D'}{D'_0}\right) \quad (24)$$

$$\frac{\hat{v}(s)}{\hat{d}(s)} = \frac{V_g}{D'^2} \frac{1 - s \frac{L}{RD'^2} \left(1 - \frac{D'}{D'_0}\right)}{1 + s \frac{L}{RD'^2} + s^2 \frac{LC}{D'^2}} \quad (25)$$

The half bridge simplification can now be justified by comparing the bode plot and step response of eq. (25) and eq. (12). For  $D' = 0.2$ ,  $R = 4 \Omega$ ,  $C = 2 \mu\text{F}$ , and  $L = 4 \mu\text{H}$ , the bode plot for the half and full bridge is plotted in fig. 8, with the corresponding step response fig. 9. It can be seen that these figures closely match, but that there are some higher-order effects that are not modelled in the half bridge simplification.

From eq. (25) it can be seen that for  $D' = D'_0$  the RHPZ disappears completely, as there is no current flowing through the inductors. In addition to that, for  $D' > D'_0$  the zero moves to the other half-plane, becoming a LHPZ. Since a full bridge consists of two half-bridges, this means that for small signals around the bias point, the LHPZ and RHPZ cancel, and the bridge configuration completely eliminates the RHPZ response.

However, this is not the case for large signal excursions. As can be seen, the

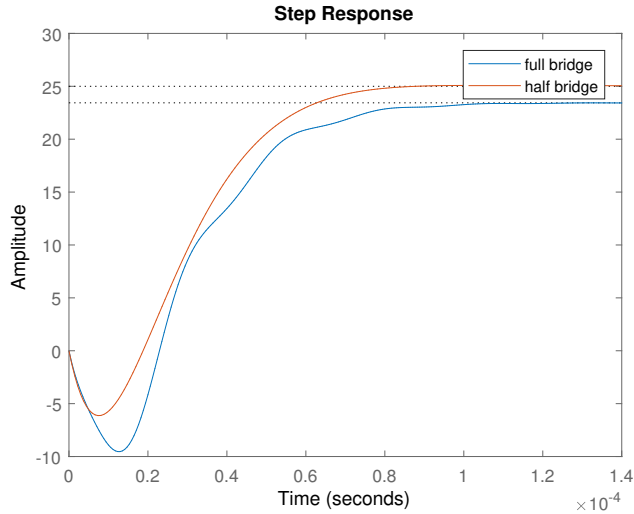


Figure 9: Step response of the full bridge and half bridge simplification

Table 1: Switching time periods with fixed forward interval

	Ground $D_{gnd}$	Freewheel $D_{free}$	Forward $D_{fwd}$
Half-bridge 1	$k_1 D$	$(1 - k_1) D$	$1 - D$
Half-bridge 2	$k_2(1 - D)$	$(1 - k_2)(1 - D)$	$D$

zero scales with  $\frac{1}{D^2}$ , meaning that the high-side half-bridge with a high duty cycle has a low-frequency RHPZ (strong inverse response), that dominates over the low-side half bridge, having a small duty cycle and a high-frequency LHPZ (weak positive response), still causing a net inverse response.

## 2.2 Tri-state boost converter

To fully eliminate the RHPZ another approach is needed. In [7] a tri-state topology is proposed that has an additional switch to loop back the inductor current on itself. It proposes a control scheme where the forward duty cycle is kept constant, and a fast transfer is achieved by varying the ground and freewheel duty cycle.

This topology is put into a bridge configuration in fig. 10 to make it suitable for audio. However, the proposed control scheme results in a high inductor current and high losses in the freewheel interval, as will be shown.

The switching intervals of the tri-state bridge in fig. 10 are summarized in table 1. Each row indicates the switching intervals for one half-bridge. The Ground column specifies the on-time of  $M_1$  or  $M_2$ , the Freewheel column refers to  $M_4$  or  $M_6$ , and the Forward column refers to  $M_3$  or  $M_5$ . So  $D$  sets the duty cycle of the bridge, while  $k_1$  and  $k_2$  control the amount of freewheel time. Unless otherwise stated, the rest of the paper discusses the half-bridge indicated by the first row.

As derived in [6] using the same method as eq. (7), the output voltage and

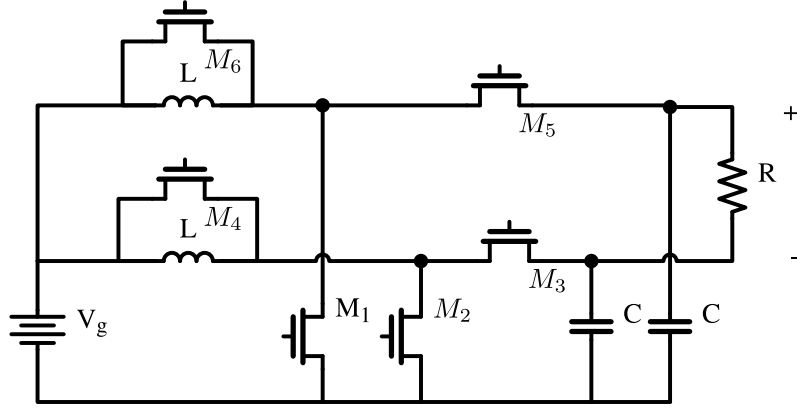


Figure 10: Bridge boost converter with inductor loop

inductor current of a single-ended tri-state boost converter is given by

$$0 = kDV_g + (1 - D)(V_g - V_R) \quad (26)$$

$$V_R = V_g \frac{kD + 1 - D}{1 - D} \quad (27)$$

$$I_L = I_R \frac{kD + 1 - D}{1 - D} \quad (28)$$

$$I_L = \frac{V_R}{R} \frac{kD + 1 - D}{1 - D} \quad (29)$$

For  $k = 1$  this is equivalent to a normal boost converter, so for normal inductor current  $I_{L,norm}$  and tri-state inductor current  $I_{L,tri}$  as derived above, this leads to the following difference in inductor current

$$\frac{I_{L,tri}}{I_{L,norm}} = 1 - D(1 - k) \quad (30)$$

When a fixed forward interval is used like in [7], the efficiency depends on the peak-to-average ratio. At peak voltage,  $k = 1$  and efficiency is optimal. For lower voltages it is shown in eq. (30) that more inductor current is required than a normal boost converter.

### 2.3 Simulation

The tri-state bridge was realized in LTspice using ideal voltage-controlled switches, comparators, and logic elements. A 1 MHz switching frequency was used. The full LTspice schematic can be found in appendix D fig. 34.

The simplified half-bridge transfer function in eq. (25) has a corner frequency of  $\omega_0 = \frac{D'}{\sqrt{LC}}$  which should be outside the audio band for all usable values of

$D'$ . An example for  $D' = 0.2$  is to take  $L = C = 1.5 \cdot 10^{-6}$ , but in simulation this gives too much switching ripple.

Ideally the full bridge equation would be used to derive correct component values, this is however a fourth order system which does not have an analytic expression for parameters such as corner frequency, damping or even poles and zeros. Instead the component values were adjusted experimentally to obtain acceptable voltage and current ripple. The values found are as follows.

$$R = 4 \Omega \tag{31}$$

$$L = 4 \mu\text{H} \tag{32}$$

$$C = 2 \mu\text{F} \tag{33}$$

As mentioned before, around the operating point no RHPZ is present. Therefore simulations are performed with a step function between positive voltages. The input signal is a step function between 3 V (60%) to 3.5 V (70%) and the forward interval is fixed at 20%.

Figure 11 plots the averaged duty cycles of the three states. It can be seen in the top plot that the ground switch (blue) follows the duty cycle directly, alternating between 60% and 70%. Except for a small averaging artifact, the forward switch duty cycle (yellow) stays constant, while the freewheel interval (red) fills in the remainder. The bottom plot is the other half bridge with opposite duty cycles.

Figure 12 plots the averaged switch currents corresponding to fig. 11, where the outer contour corresponds to the inductor current. A key moment is at 5 ms, where a decrease in duty cycle occurs. Normally the instant increase of forward on-time combined with the slowly decreasing inductor current, creates a current spike. However, in this graph it can be seen that the freewheel current makes a spike, while the forward current only decreases. Note however, the large amount of freewheel current (red).

Figure 13 shows the output voltage of the circuit, and shows that indeed no inverse RHPZ response is present.

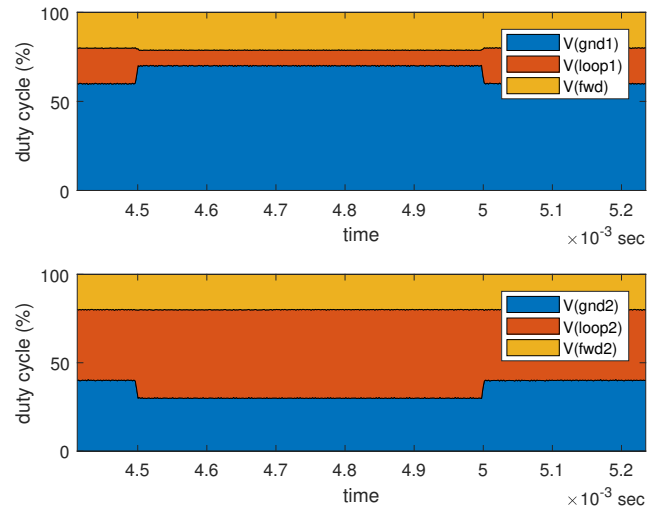


Figure 11: Area plot of averaged duty cycle with fixed forward interval

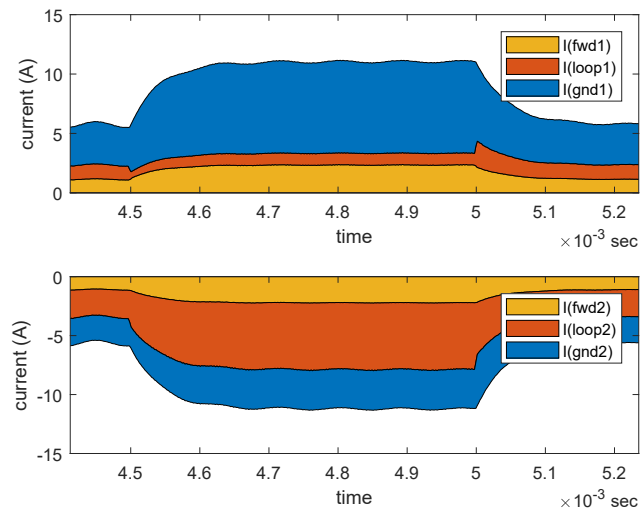


Figure 12: Area plot of averaged switch currents with fixed forward interval

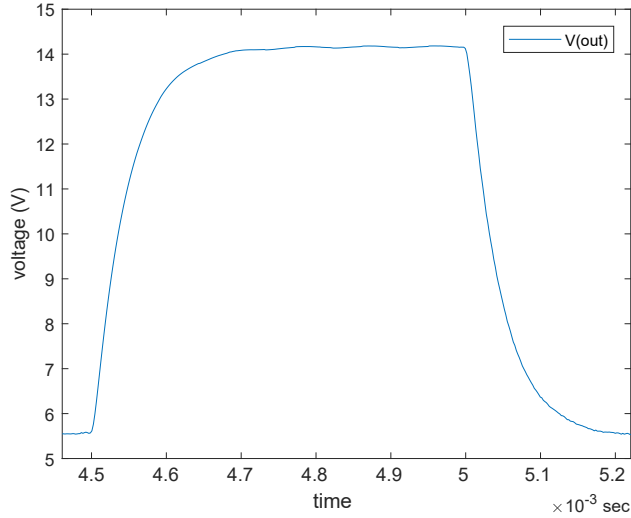


Figure 13: Output voltage with fixed forward interval

### 3 Dynamic Tri-state Bridge Boost Converter

So far, it has been found that combining two approaches from the literature, namely a bridge configuration combined with a tri-state topology provides excellent performance suitable for audio applications. However, it was shown that efficiency is worse than a normal boost converter bridge.

To achieve better efficiency, the freewheel interval should be dynamically controlled to be as small as possible without introducing RHPZ behavior. The root cause of the RHPZ response is that the forward interval is reduced faster than the inductor current is increased, causing a reduced forward current. So the key design goal is to limit fast changes to the forward interval.

Going forward with a more convenient notation from table 2: The idea is to control the freewheel interval  $p$  by applying a biased high-pass filter to  $D$ , such that in steady state, a set amount of excess current is present in the inductor.

In the following example, the effect of applying a high-pass filter will be demonstrated by applying a step function  $u(t)$  of  $\Delta D$  to a system with duty cycles  $D_{gnd}$ ,  $D_{free}$  and  $D_{fwd}$  as defined in table 2, in a steady-state situation set by  $D_0$ , and  $p_0$ . For simplicity, the control of  $p$  is taken to be a first-order high-pass filter with time constant  $\tau$ .

Table 2: Switching time periods for a dynamic freewheel interval

	Ground $D_{gnd}$	Freewheel $D_{free}$	Forward $D_{fwd}$
Half-bridge 1	$D$	$p_1$	$1 - D - p_1$
Half-bridge 2	$1 - D$	$p_2$	$D - p_2$

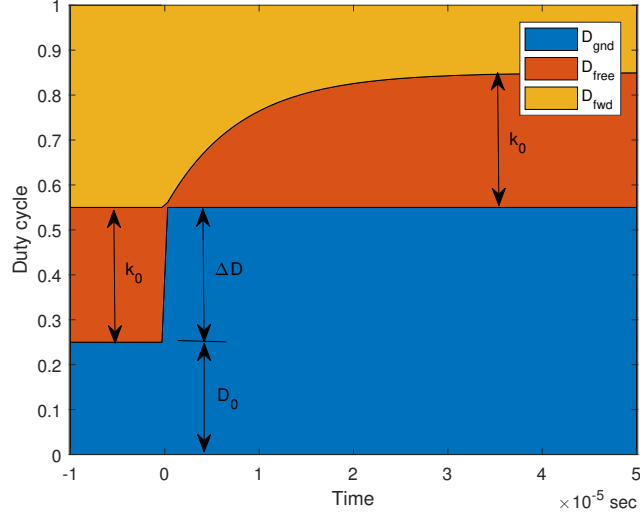


Figure 14: Example step response duty cycles

$$D_{gnd}(t) = D(t) = D_0 + u(t)\Delta D \quad (34)$$

$$D_{free}(t) = p(t) = p_0 - u(t)\Delta D e^{-\frac{t}{\tau}} \quad (35)$$

$$D_{fwd}(t) = 1 - D(t) - p(t) \quad (36)$$

$$D_{fwd}(t) = 1 - D_0 - u(t)\Delta D - p_0 + u(t)\Delta D e^{-\frac{t}{\tau}} \quad (37)$$

$$D_{fwd}(t) = 1 - D_0 - p_0 - u(t)\Delta D(1 - e^{-\frac{t}{\tau}}) \quad (38)$$

This results in the following initial and final conditions.

$$D_{free}(0) = p_0 - \Delta D \quad (39)$$

$$D_{free}(\infty) = p_0 \quad (40)$$

$$D_{fwd}(0) = 1 - D_0 - p_0 \quad (41)$$

$$D_{fwd}(\infty) = 1 - D_0 - p_0 - \Delta D \quad (42)$$

An example step response for the above equations is displayed in fig. 14, where an instantaneous change in duty cycle  $D = D_{gnd}$ , results in a gradual change in the forward interval  $D_{fwd}$ . From this graph it becomes obvious that an instantaneous step of  $\Delta D > p_0$  can not be fully compensated.

Since the audio input is generally band-limited to 20 kHz, this puts a limit on the slope of the duty cycle of  $\frac{dD(t)}{dt} \leq \frac{1}{\pi 40000}$ , where most energy is concentrated in lower frequencies. So it is expected that a relatively small  $p$  margin will produce good results in most cases except sharp, full-swing transients.

### 3.1 High-pass filter design

It was shown that by controlling the freewheel duty cycle with a high-pass filter, the forward interval effectively sees low-pass behavior. This is important because too fast changes in forward duty cycle lead to an inverse response.

To design a high-pass filter a trade-off is made between efficiency and frequency response. If the filter is given a very low cut-off frequency it behaves almost as a fixed-forward boost converter. If the frequency is chosen too high, the RHPZ is not fully compensated because the forward duty cycle changes faster than the inductor current.

To obtain a non-inverted step response, it is required that for a positive input step, the derivative of the average forward switch current  $I_{fwd}$  is also positive. As is shown below, this means that the derivative of the inductor current  $I_L$  has to be larger than the derivative of the forward duty cycle  $D_{fwd}$  as defined in table 2.

$$D_{fwd} = 1 - D - p \quad (43)$$

$$I_{fwd} = D_{fwd} \cdot I_L \quad (44)$$

$$\frac{dI_{fwd}}{dt} = \frac{dD_{fwd}}{dt} I_L + D_{fwd} \frac{dI_L}{dt} \quad (45)$$

$$\frac{dI_{fwd}}{dt} > 0 \quad (46)$$

$$\frac{\frac{dI_L}{dt}}{I_L} > \frac{-\frac{dD_{fwd}}{dt}}{D_{fwd}} \quad (47)$$

$$\frac{\frac{dI_L}{dt}}{I_L} > \frac{\frac{dp}{dt} + \frac{dD}{dt}}{D_{fwd}} \quad (48)$$

Using a first order RC filter to control  $p$  is undesirable as will be shown. By applying a step function to the filter ( $\frac{1}{s}$ ), taking the derivative ( $s$ ), and applying the initial value theorem, the initial slope of a first and second order filter  $H_{1st}$  and  $H_{2nd}$  with arbitrary cut-off frequency  $\omega_0$  and quality factor  $Q$  are as follows.

$$\mathcal{L}\{y'(t)\} = \frac{s}{s} H(s) \quad (49)$$

$$\lim_{t \rightarrow 0} y'(t) = \lim_{s \rightarrow \infty} sH(s) \quad (50)$$

$$H_{1st}(s) = \frac{1}{1 + \frac{s}{\omega_0}} \quad (51)$$

$$\lim_{t \rightarrow 0} y'_{1st}(t) = \lim_{s \rightarrow \infty} \frac{s}{1 + \frac{s}{\omega_0}} \quad (52)$$

$$y'_{1st}(0) = \omega_0 \quad (53)$$

$$H_{2nd}(s) = \frac{\omega_0^2}{s^2 + s\frac{\omega_0}{Q} + \omega_0^2} \quad (54)$$

$$\lim_{t \rightarrow 0} y'_{2nd}(t) = \lim_{s \rightarrow \infty} \frac{s\omega_0^2}{s^2 + s\frac{\omega_0}{Q} + \omega_0^2} \quad (55)$$

$$y'_{2nd}(0) = 0 \quad (56)$$

Due to the  $LC$  tank in fig. 6, the inductor current  $I_L$  has a second order response. This means that a first-order filter can not satisfy eq. (48) and obtain a strictly positive response. By using a second order filter, a much faster response can be obtained while still resulting in a strictly positive derivative of the average forward switch current. However, care must be taken when designing the high-pass filter to properly match the inductor current response.

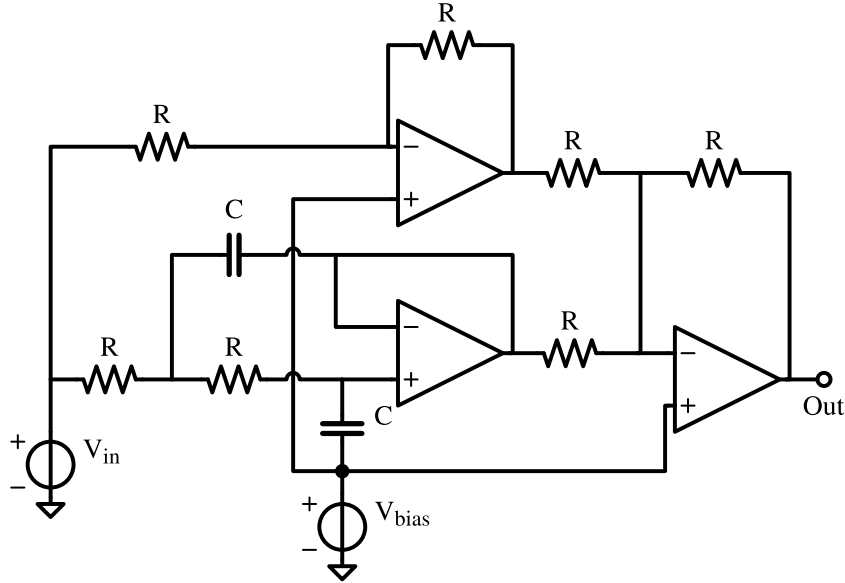


Figure 15: Modified Sallen-Key high-pass filter

It was discussed that the forward interval sees an effective low-pass filter corresponding to the high-pass filter on the freewheel interval. However, for a second order filter this does not give the desired behaviour. The high-pass filter corresponding to the desired low-pass filter is as follows (notice the extra  $s$  term in the numerator compared to a normal high-pass filter)

$$H_{LP}(s) = \frac{\omega_0^2}{s^2 + s\frac{\omega_0}{Q} + \omega_0^2} \quad (57)$$

$$H_{HP}(s) = 1 - \frac{\omega_0^2}{s^2 + s\frac{\omega_0}{Q} + \omega_0^2} \quad (58)$$

$$H_{HP}(s) = \frac{s^2 + s\frac{\omega_0}{Q}}{s^2 + s\frac{\omega_0}{Q} + \omega_0^2} \quad (59)$$

This filter can either be implemented using a biquad filter structure, or a direct implementation using a low-pass filter and an opamp adder. The latter was chosen due to simplicity of the filter design. The implementation is drawn in fig. 15.

### 3.2 PWM generation

Since traditional PWM generators have only two states, a new circuit is required. To realize three states, two comparators are used, as in fig. 16. The first comparator is connected to  $V_{in}$  and  $V_{triangle}$  and the second is connected to the high-pass filtered  $h(V_{in})$  and  $V_{triangle}$ . The outputs of the comparators

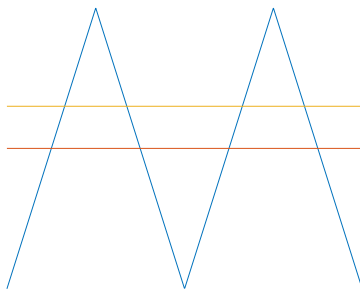


Figure 16: Example comparator inputs  $V_{in}$ ,  $h(V_{in})$ ,  $V_{triangle}$

Table 3: Tri-state truth table

$\mathcal{D}$	$\mathcal{P}$	$gnd$	$fwd$	$loop$
1	1	1	0	0
0	1	0	0	1
1	0	1	0	0
0	0	0	1	0

then form two state variables  $\mathcal{D} = V_{in} > V_{triangle}$  and  $\mathcal{P} = h(V_{in}) > V_{triangle}$  that correspond to the duty cycles  $D$  and  $p$ .

The final PWM signals can then be realized using Boolean logic. To derive the needed logic, a truth table was made, shown in table 3. When  $\mathcal{D}$  the inductor is charged as usual, but when  $\neg\mathcal{D}$  it depends on  $\mathcal{P}$  if the output is charged or the inductor looped back on itself.

$$gnd_1 = \mathcal{D} \tag{60}$$

$$fwd_1 = \neg\mathcal{D} \wedge \neg\mathcal{P}_1 \tag{61}$$

$$loop_1 = \neg\mathcal{D} \wedge \mathcal{P}_1 \tag{62}$$

$$gnd_2 = \neg\mathcal{D} \tag{63}$$

$$fwd_2 = \mathcal{D} \wedge \neg\mathcal{P}_2 \tag{64}$$

$$loop_2 = \mathcal{D} \wedge \mathcal{P}_2 \tag{65}$$

A high-level realization of this circuit is pictured in fig. 17. In a real-world application, a small addition is needed to add dead-time. Rather than implementing 3-way dead-time, a simple circuit was designed that delays the rising edge of each switch, shown in fig. 18. A complete low-level implementation of the filter and logic can be found in appendix D fig. 34.

### 3.3 Simulation

The same circuit and input are used to test the proposed control method as were used in section 2.3: A step function from 3 V (60%) to 3.5 V (70%). The

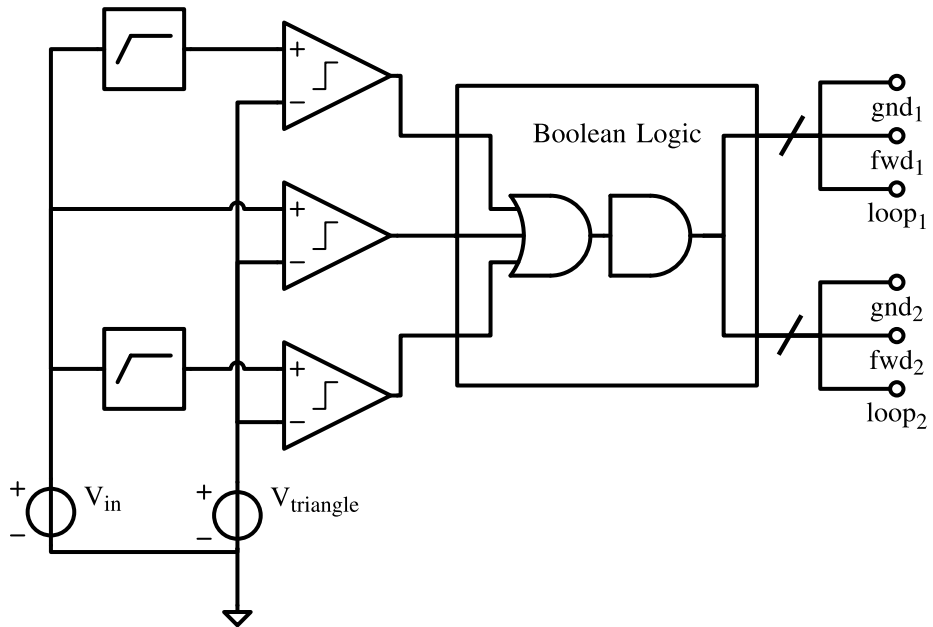


Figure 17: Tri-state PWM schematic

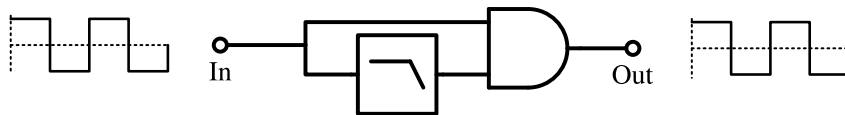


Figure 18: Rising edge delay (pseudo dead time) schematic

freewheeling interval is driven by a second order high-pass filter with a cut-off of 8 kHz, biased around 10% duty cycle.

Figure 19 plots the averaged duty cycles of the three states. Compared to fig. 11, the forward switch duty cycle (yellow) can be seen to change with a gradual curve from the second-order filter, while the freewheel interval (red) always returns to 10% duty cycle.

Figure 20 plots the averaged switch currents corresponding to fig. 19. Similar to fig. 12 it can be seen that the freewheel interval makes a current spike, while the forward current only decreases. Note that the amount of freewheel current is much lower than in fig. 12.

Figure 21 shows the output voltage of the circuit, and shows that again no inverse RHPZ response is present. Some slight ringing is present, caused by the underdamped response of the low-side half-bridge, seen in the bottom plot of fig. 20 and fig. 9.

With a second order filter, the cut-off frequency could be increased to 8 kHz without introducing a noticeable inverted response. This is 5 times higher than was possible with an RC filter, and provides a much faster step response. The output from a 1.5 kHz RC filter is plotted in fig. 22.

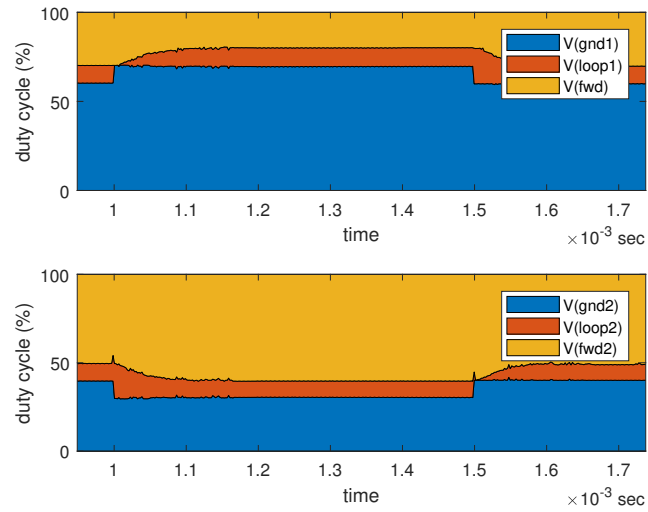


Figure 19: Averaged duty cycle with 8 kHz Sallen-Key filter

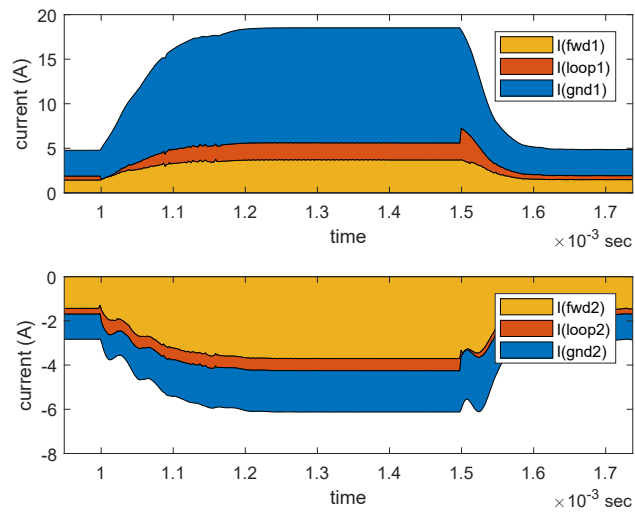


Figure 20: Averaged switch currents with 8 kHz Sallen-Key filter

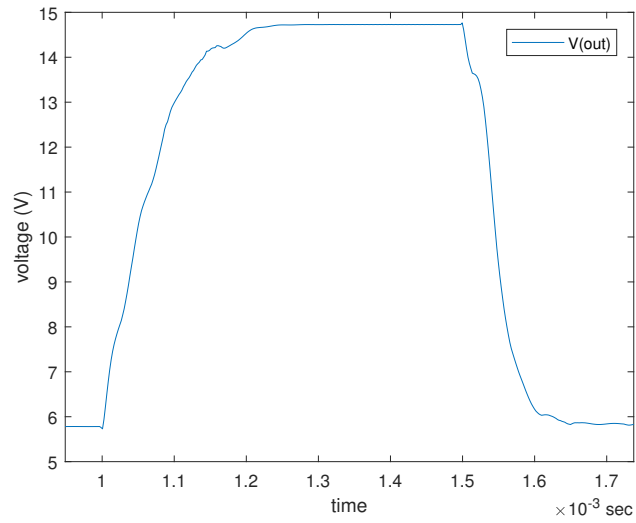


Figure 21: Output voltage with 8 kHz Sallen-Key filter

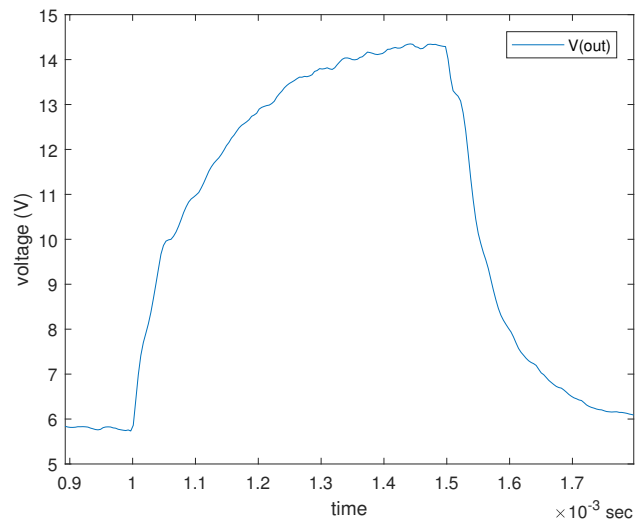


Figure 22: Output voltage with 1.5 kHz RC filter

## 4 Discussion

In isolation the proposed control scheme appears to work quite well, however, the question should be asked if it actually improves over other approaches.

Removing the freewheeling switch completely, the normal step response can be seen in fig. 23. Compared to figs. 13 and 21, the response is much steeper, much less damped, and has the characteristic RHPZ. The maximum inductor current is 16 A, compared to 18.5 A for the proposed method. So it is safe to say that if the RHPZ is not a problem, an uncompensated bridge provides the best performance.

### 4.1 Feedback stability

The theory is that by removing the RHPZ, more open loop gain can be applied without causing phase reversal at higher frequencies. To test this theory, a feedback loop was added around 3 variations of the boost converter bridge. No extensive compensator design was done, using only a simple voltage feedback system with 10 times attenuation. The circuit can be found in appendix D figs. 34 and 36.

This was done for a boost converter without compensation, a boost converter with a fixed forward interval, and the proposed dynamic freewheeling interval. For each circuit, the open loop gain was increased until instability occurred. Then for the maximum open loop gain, the THD was measured at 1 kHz, resulting in table 4.

It was found that for the dynamic freewheeling circuit the possible loop gain depends on the freewheel margin as well as the cut-off frequency. In this test a cut-off of 8 kHz was used with  $p = 0.2$ . For  $p = 0.1$  a gain of 4 was possible.

### 4.2 Parameter Sweep

The proposed method allows adjusting the amount of freewheel current and the steepness of the step response. As the high-pass filter cut-off frequency approaches  $\infty$  Hz, the circuit reduces to a normal boost converter, while letting the high-pass filter cut-off frequency approach 0 Hz reduces to having a fixed forward duty cycle. The amount of freewheel duty cycle in steady state determines the maximum compensated voltage swing.

A 10 kHz sine of 1 V was applied to the boost converter while varying the high-pass filter cut-off frequency. In fig. 24 the THD was plotted for each frequency, showing a sharp cliff at 5 kHz. Corresponding output voltages are shown in fig. 25.

It should be note that the freewheel margin was kept constant for all cases, which is not the typical configuration for the extremes where the circuit reduces to either a normal boost converter or a boost converter with a fixed forward

Table 4: Feedback performance at 1 V amplitude, 1 kHz

	Gain	THD (%)
Standard	1	1.16
Dynamic	5	0.53
Fixed forward	13	0.11

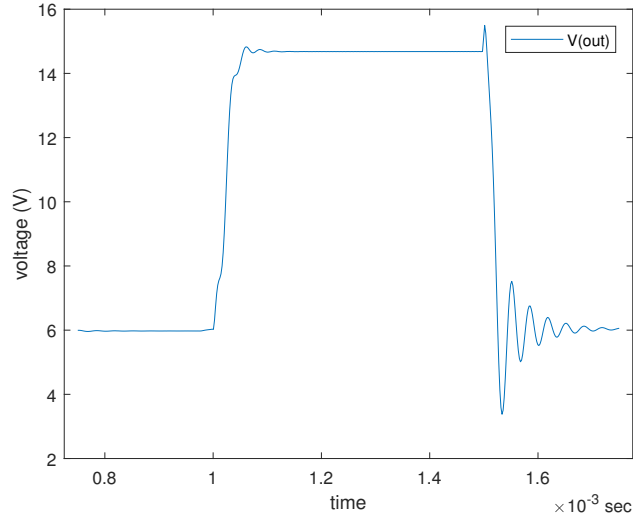


Figure 23: Output voltage of normal boost converter bridge

interval. This means that for  $\infty$  Hz, freewheel current is wasted at no real benefit, while at 0 Hz the voltage swing is strictly limited by the set freewheel margin.

### 4.3 Efficiency

The premise of the dynamic freewheeling design is that it improves efficiency. Therefore a discussion would not be complete without something to back up this claim. However, a few challenges exist when attempting to quantify the efficiency of the different schemes. For both the fixed forward interval and the dynamic freewheeling schemes there are some parameters that influence efficiency.

For the fixed forward interval scheme, efficiency mainly depends on the maximum output voltage and the peak-to-average ratio of the signal. As can be seen from eq. (30), a high peak-to-average ratio reduces efficiency, so a sine wave or square wave would give an optimistic estimate of efficiency.

For the dynamic freewheeling scheme, quality depends on the filter cut-off, but efficiency depends mainly on the freewheel margin. This is dictated by the filter cut-off and frequency spectrum of the signal. In most music the amplitude of high frequencies is low, allowing a small freewheel margin. In this case a sine wave or square wave will put unrealistic demands on the freewheel margin and produce a pessimistic estimate.

Rather than trying to device a test signal that mimics real music in both frequency spectrum and peak-to-average ratio, a 1 s section of Sultans of Swing by Dire Straits was used.

An exhaustive and realistic comparison is difficult, if not impossible to carry out. Due to the different transfer functions of the circuits it is already impossible to get the same output out of all three circuits. Furthermore, the efficiency

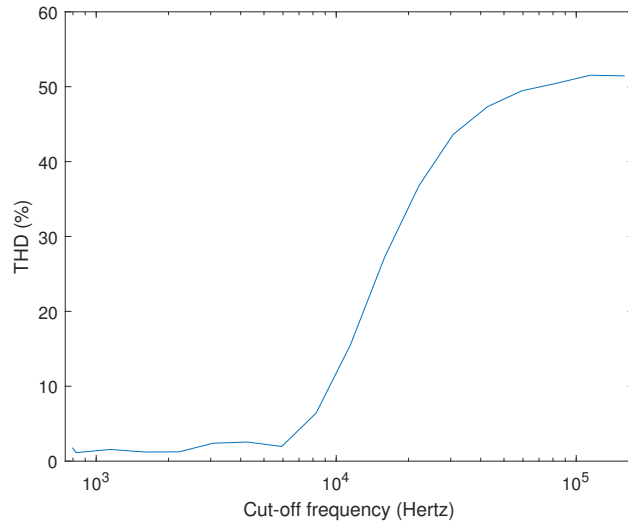


Figure 24: THD of a 1 V 10 kHz sine wave for various high-pass cut-off frequencies

Figure 25: Output voltage for a given cut-off frequency

	Input (W)	Output (W)	Efficiency (%)	$I_{L,1} + I_{L,2}$ (A)
Standard	2.0	1.6	82.5	1.52 + 1.54
Dynamic	1.6	1.2	75.3	1.53 + 1.58
Fixed	3.7	2.0	55.1	3.63 + 3.69

greatly depends on real-world parasitic losses, which are not fully modelled.

In table 5 the RMS input and output power are displayed for a 1 s sample of Sultans of Swing by Dire Straits. The same parameter values were used as in the other simulations. It can be seen that for a comparable output power, the inductor current is indeed larger for the dynamic converter than the standard bridge, and larger still for the fixed forward converter. This directly translates to parasitic losses, reflected in the efficiency.

In all simulations, switch on resistance is 10 m $\Omega$ , inductor resistance is 5 m $\Omega$ , other parasitics are not modelled. So it may be expected that real-world losses are different from what is shown here. The inductor currents should give a relative measure of efficiency.

## 5 Conclusion

The goal of this report was to investigate ways to eliminate the RHPZ response from a boost converter control-to-output transfer. It was found that a bridge configuration removes direct current, is more linear, cancels out even-order distortion, and reduces RHPZ behavior.

To fully remove the RHPZ, the bridge was combined with a tri-state topology. This combination is suitable for audio and completely eliminates the RHPZ. However, it was shown that a control scheme with a fixed forward interval reduces efficiency.

A normal boost converter in bridge has a sharp step response, but exhibits RHPZ behavior, while a fixed forward duty cycle contains no RHPZ at the expense of a slower step response and high freewheel current. A new control scheme was proposed that provides a trade-off between freewheel current losses and frequency response. The new scheme can compensate the RHPZ under most circumstances and is more efficient than using a fixed forward duty cycle.

It was found that using a simple voltage feedback loop, a higher loop gain could be achieved than a standard boost converter, and that freewheel current can be traded off for extra loop gain. Up to 13 times more loop gain was possible with a completely fixed forward duty cycle compared to a bare bridge boost converter. With a freewheel duty cycle of 10%-20% and cut-off of 8 kHz, gains of 4-5 times that of the basic configuration are possible.

Efficiency was measured using a short audio sample, and it was found that with the chosen simulation parameters, the proposed scheme is about 20 p.p. more efficient than a boost converter with a fixed forward duty cycle, and 7 p.p. less efficient than a boost converter without compensation.

So it has been demonstrated that a dynamic tri-state boost converter has a THD of less than one percent and an efficiency that is expected to be in the same ballpark as the combination of a boost converter and class-D amplifier. While

further testing and fine-tuning is needed, this demonstrates that this approach is a viable alternative for low-voltage portable audio applications.

## References

- [1] Thomas Haagen Birch et al. “Predistortion of a Bidirectional Cuk Audio Amplifier”. In: *Audio Engineering Society Convention 137*. Oct. 2014. URL: <http://www.aes.org/e-lib/browse.cfm?elib=17515>.
- [2] R.W. Erickson and D. Maksimovic. *Fundamentals of Power Electronics*. Power electronics. Springer US, 2001. ISBN: 9780792372707.
- [3] F. A. Himmelstoss, J. W. Kolar, and F. C. Zach. “Analysis of a Smith-predictor-based-control concept eliminating the right-half plane zero of continuous mode boost and buck-boost DC/DC converters”. In: *Industrial Electronics, Control and Instrumentation, 1991. Proceedings. IECON '91., 1991 International Conference on*. Oct. 1991, 423–428 vol.1. DOI: 10.1109/IECON.1991.239347.
- [4] Gert Bolten Maizonave et al. “Double-Boost DC-AC Converter with Sliding-Mode Control for Portable Audio”. In: *Audio Engineering Society Conference: 37th International Conference: Class D Audio Amplification*. Aug. 2009. URL: <http://www.aes.org/e-lib/browse.cfm?elib=15212>.
- [5] V. Michal. “Modulated-Ramp PWM Generator for Linear Control of the Boost Converter’s Power Stage”. In: *IEEE Transactions on Power Electronics* 27.6 (June 2012), pp. 2958–2965. ISSN: 0885-8993.
- [6] V. Michal, D. Cottin, and P. Arno. “Boost DC/DC converter nonlinearity and RHP-zero: Survey of the control-to-output transfer function linearization methods”. In: *2016 International Conference on Applied Electronics (AE)*. Sept. 2016, pp. 1–10. DOI: 10.1109/AE.2016.7577229.
- [7] K. Viswanathan, R. Oruganti, and D. Srinivasan. “A novel tri-state boost converter with fast dynamics”. In: *IEEE Transactions on Power Electronics* 17.5 (Sept. 2002), pp. 677–683. ISSN: 0885-8993. DOI: 10.1109/TPEL.2002.802197.

## 6 Appendix

### A Single-ended dynamic predistortion

Before even starting the analysis, an experiment was performed where a step function was predistorted by hand-tuning the input. fig. 26 shows a Simulink simulation where the middle graph shows a hand-tuned exponential, while the top graph shows the output voltage. The bottom graph shows the input current. As can be seen the current starts increasing while the output voltage is kept constant, and the output only starts changing when the exponential ends.

This was a very promising start, but further analysis revealed it was hardly applicable. As derived in eq. (19), the RHPZ is heavily dependant on the duty cycle, meaning the predistortion also depends on the duty cycle.

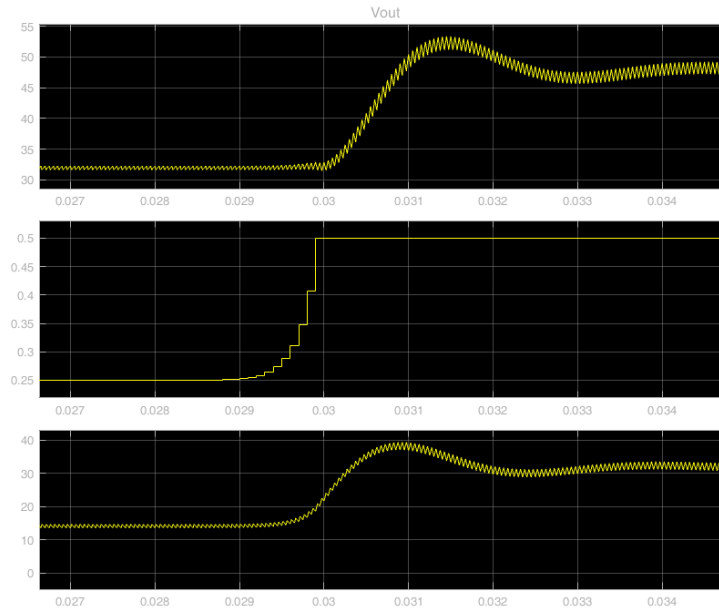


Figure 26: Predistortion of a step function

Furthermore, the intended application is audio, where a direct current through the driver is undesirable or even dangerous. Therefore some decoupling is required. However, this completely changes the transfer function, further complicating analysis.

And finally, it does not solve the problem of feedback instability. In the end it is desirable to have feedback, but since the predictor is based on future data, it can not incorporate feedback. This means that the RHPZ is still present in the feedback loop, limiting the loop gain severely.

Related paper: [3]

## B Static bridge Predistortion

In [5] an approach is presented that predistorts the PWM signal with  $\frac{1}{1-D}$  by modulating the slope of the triangle wave. While this approach could be applied twice for each half of the bridge, it was found that the dynamic behavior of this approach is worse than predistorting the total bridge behavior.

An approach for predistorting a bridge configuration was presented in [1]. This approach relies on a linear region and a quadratic region, approximated by a MOSFET. Practical challenges were met matching the MOSFETs to achieve good performance.

The approach presented here relies on distorting the triangle wave in yet another way based on the following insight. A triangle wave corresponds to a linear relation between the input voltage and the duty cycle. If the triangle were a periodic signal shaped according to  $V_R = \frac{1-2D}{D-D^2}$ , the duty cycle would be the inverse relation, leading to a linear output voltage.

It is theorized that if an integrator was used to obtain the triangle from a square wave, there exists a filter that will produce the desired predistortion.

$$G(s) = H(s)F(s) \quad (66)$$

$$\frac{G(s)}{F(s)} = H(s) \quad (67)$$

However, a direct solution is tedious and unlikely to produce a realizable result because the theoretical output voltage goes to infinity for  $D = 1$  and  $D = 0$ .

Instead the problem was approached from the other direction: What kind filter would have a response close to what is desired? By inspection it appears some sort of high-pass behavior is desired. Some experimentation revealed that an undamped second order high-pass filter produces a useful sine when the cut-off frequency is taken at twice the triangle frequency. When attenuated by a factor  $G$  and summed with an all-pass it gives the result in fig. 27.

Since this is a normal second order filter and an all-pass filter, it can be easily implemented as an LC filter and an adder, as done in fig. 28. Alternatively a Sallen-Key topology could be used to eliminate the inductor.

$$f_{triangle} = 1 \text{ MHz} \quad (68)$$

$$\omega_0 = 4\pi f_{triangle} \quad (69)$$

$$Q \gg 1 \quad (70)$$

$$H(s) = 1 + G \frac{s^2}{s^2 + s \frac{\omega_0}{Q} + \omega_0^2} \quad (71)$$

$$H(s) = \frac{s^2(1 + G) + s \frac{\omega_0}{Q} + \omega_0^2}{s^2 + s \frac{\omega_0}{Q} + \omega_0^2} \quad (72)$$

The proposed filter was implemented in LTspice, and the output of a boost converter bridge with and without this predistortion filter was plotted in fig. 29.

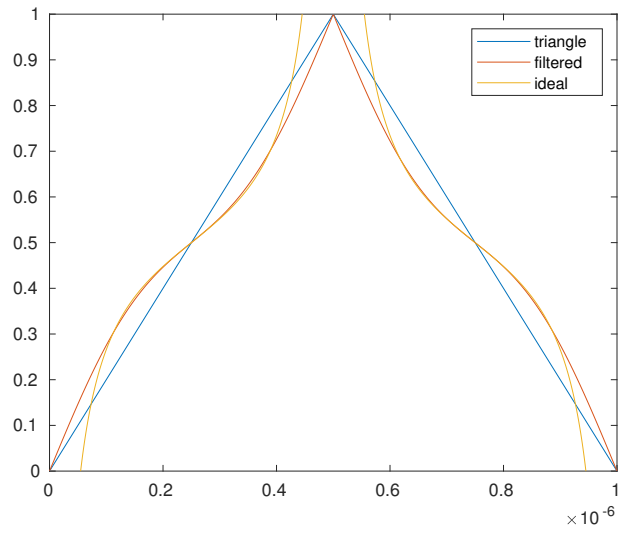


Figure 27: Comparison of ideal predistortion and filter output

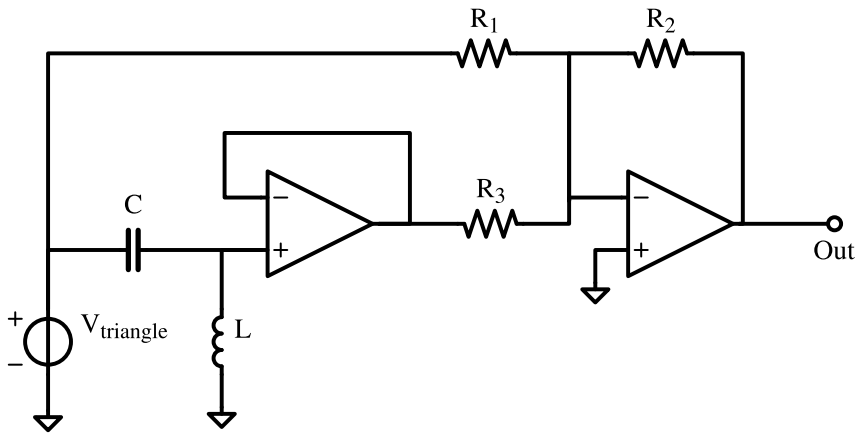


Figure 28: Opamp implementation of proposed predistortion

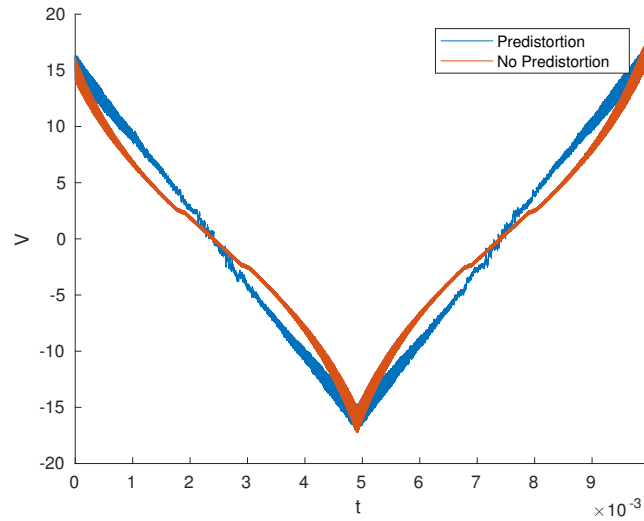


Figure 29: Output voltage with and without predistorted triangle wave

## C Peak detector

A challenge with the approach in [7] is setting the correct forward duty cycle. Not only does this limit the maximum output voltage, setting the maximum too high wastes a lot of power in the freewheel interval in low voltages. An optimal response is achieved when the maximum output voltage perfectly envelopes the input signal.

A simple way to do this is to put a peak detector on the comparator driving the forward interval, as in fig. 35. Running the same simulation as before on this circuit produces exceptionally good results, as can be seen in figs. 30 to 32. However, this is not a fair comparison as the peak detector is optimal in this highly synthetic scenario. In realistic signals, more current will be wasted, and sharp transients may not be fully compensated.

An improvement for real music from a stored digital source would be to "look into the future" and perfectly predict the required envelope. Unlike predistortion, this approach would be fully compatible with high levels of feedback.

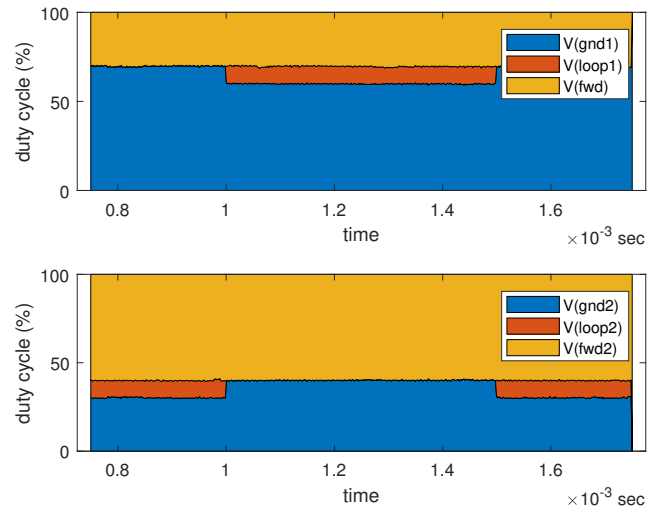


Figure 30: Averaged duty cycle with peak detector

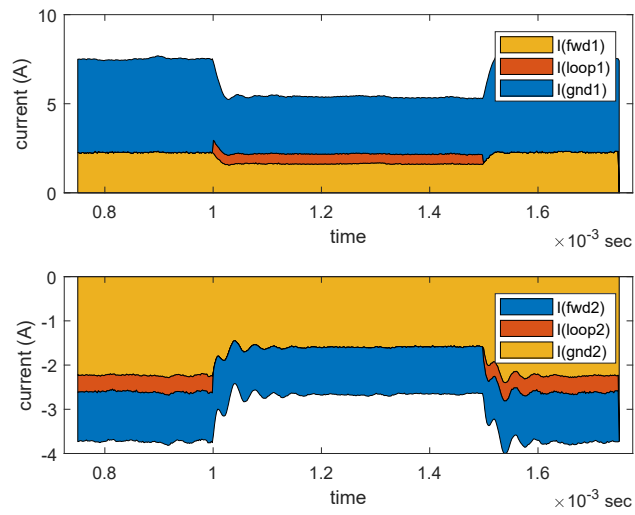


Figure 31: Averaged switch currents with peak detector

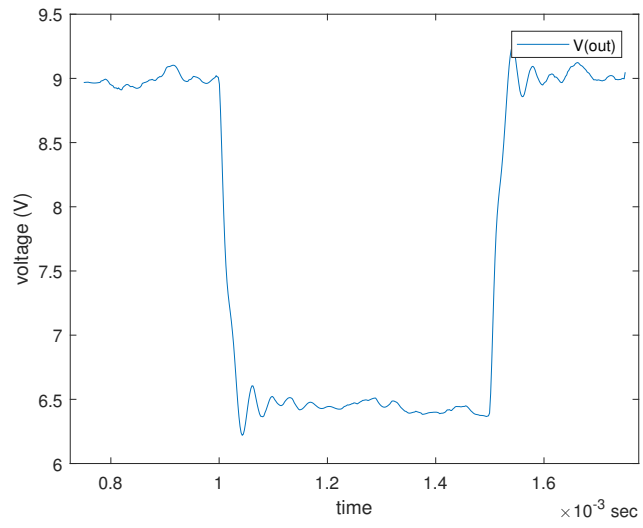


Figure 32: Output voltage with peak detector

## D LTspice schematics

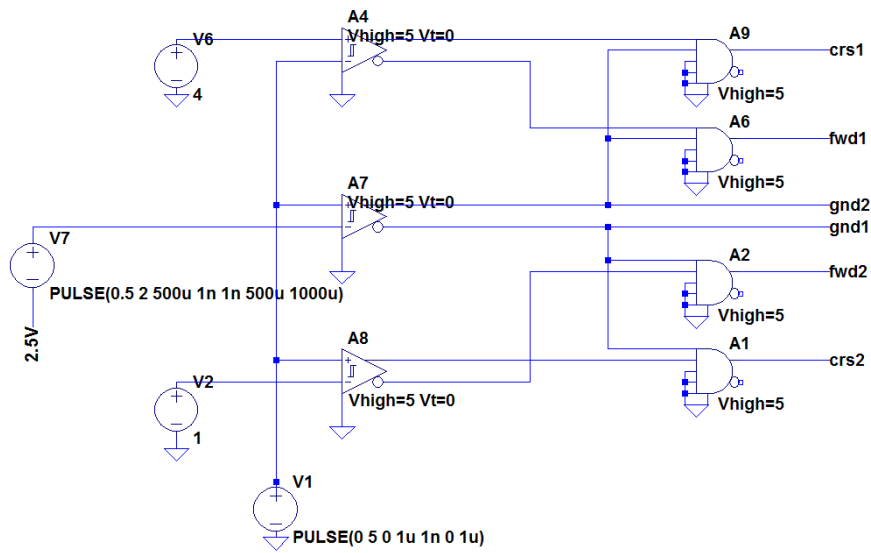


Figure 33: PWM schematic with fixed forward interval

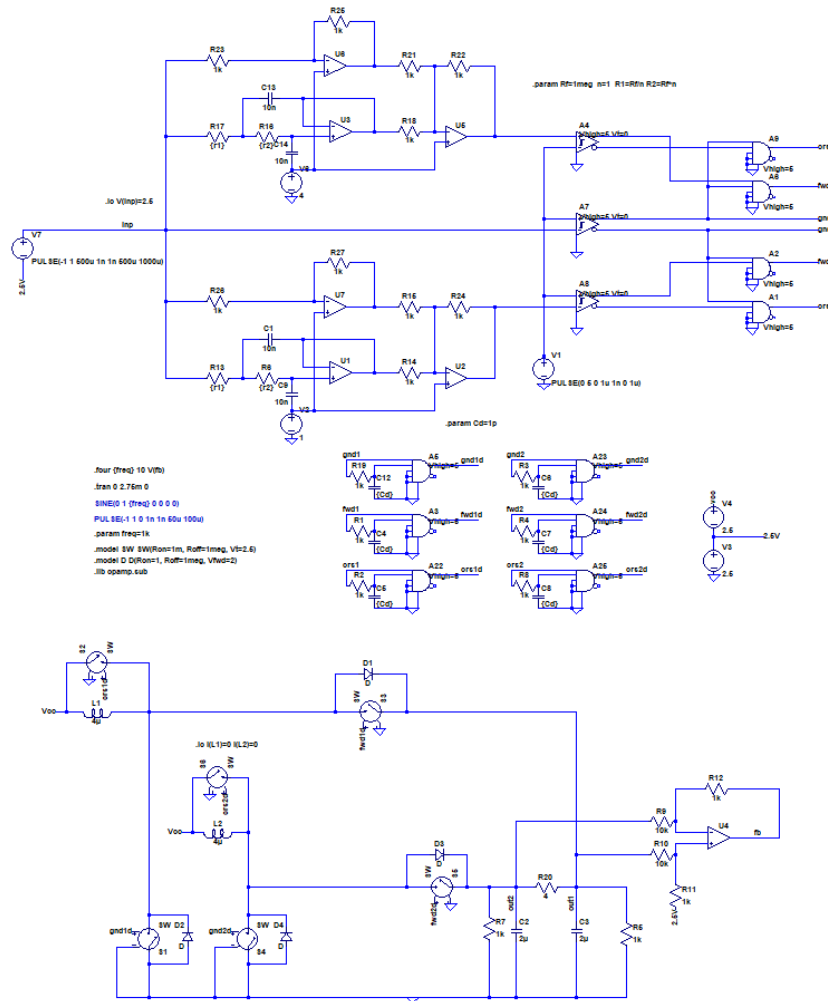


Figure 34: Complete LTspice schematic of dynamic tri-state bridge

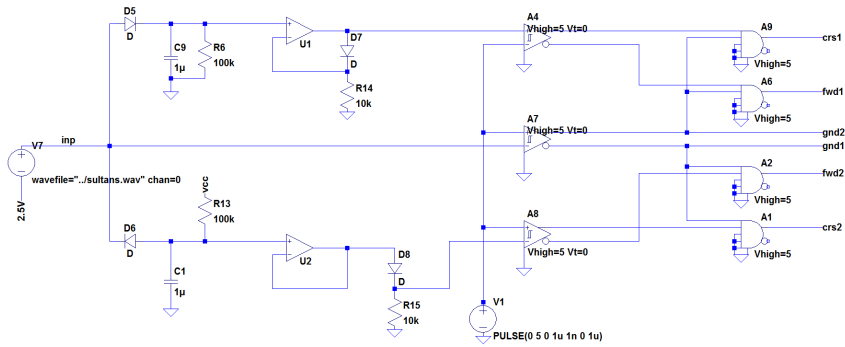


Figure 35: PWM schematic with peak detector

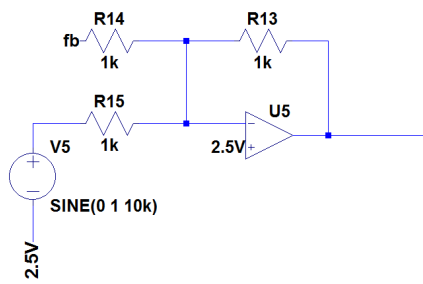


Figure 36: Feedback adder connected to fb in fig. 34